Materials and Devices
An International Scientific Journal
OPEN ACCESS
Freely Accessible Scientific Papers.
CA-IP
Managed by scientists for Science - http://co-ac.com

Article type: A-Regular research paper

Insight into negative trions binding energy behavior inside type-I and reversed type-I core/shell quantum dots: A variational analysis

A. Chafai (1,*), I. Essaoudi (1), A. Ainane (1), C. A. Duque (2)

(1) Laboratoire de Physique des Matériaux et Modélisation des Systèmes, (LP2MS), Unité Associée au CNRST-URAC 08, University of Moulay Ismail, Physics Department, Faculty of Sciences, B.P. 11201, Meknes, Morocco
(2) *Grupo de Materia Condensada-UdeA, Instituto de Fisica, Facultad de Ciencias Exactas y Naturales, Universidad de Antioquia UdeA, Calle 70 No. 52-21, Medellin, Colombia*

***Corresponding author : a.chafai@edu.umi.ac.ma**

RECEIVED: 01 June 2023 / RECEIVED IN FINAL FORM: 19 August 2023 / ACCEPTED: 04 September 2023

Abstract : Many body interactions between single particles inside low-dimensional semiconducting materials play a critical role in their optical characteristics. Within this context, tuning trionic and excitonic binding energy enables tailoring of the optical band gap of a given material. In this paper, we theoretically investigated the binding energy (E_b) of negatively charged excitons inside GaN/AlN type-I, and AlN/GaN inverted type-I core/shell quantum dots. Firstly, we started our study by examining the variation in the energy of electrons (holes) according to the change in the internal and external radii – as a means to obtain an insight into the energetic behavior of non-correlated single particles inside the two understudied nanosystems. The feature of the radial probability density distribution of confined single particles and negative trions is also discussed. Afterwards, we examined the impact of the heteronanodot spatial parameters (core radius and shell thickness) on the binding energy of confined trions. A comparison between the E_b behavior of negative trions inside core/shell type-I, and reversed type-I nanodots is also highlighted. Our results exhibit a strong dependence of the negative trion binding energy on the core material size and the shell thickness, and on the core-to-shell band mismatch as well. The obtained data also show the opportunity of modulating the negatively charged exciton correlation energy in a broad range extending from 220 to 650 meV. That paves the way for new optoelectronic devices based on III-Nitride core/shell quantum dots.

Keywords : Charged-excitons; Core/shell materials; Binding energy; Size effect; Nitride-based quantum dots

Introduction

Nowadays, III-Nitride based materials are perceived as one of the most important families of semiconductor materials after Silicon [1, 2, 3]. Indeed, Nitride semiconductors have become very useful in optic and electronic devices. That is mainly coming down from their ability to absorb/radiate radiation with wavelength extending from 200 nm (Ultraviolet) to 540 nm (green), and their capability to operate under very harsh conditions (high temperature, high power level, etc). Thus, III-Nitride materials are very attractive in various fields of applications including consumer electronics [4], lighting and displays [5], high-power RF/switching devices [6], quantum information technology [7, 8], and so many other quantum optical appliances [9, 10, 11]. The foregoing are just some examples of appliances of Nitride materials. The further application of this kind of semiconductors, operating in a very hostile environment might revolutionize the industry of electronic and optoelectronic devices.

Over the last few decades, the investigation of the properties of nanoscale Nitride-based materials, more particularly III-Nitride quantum dots (QD) [12] and Nitride monolayer materials [13, 14], has attracted considerable attention on the part of the material sciences researcher-community. That is, to a large extent, motivated by the unique properties of Nitride semiconductors, namely their wide energy bandgap, large excitonic effects, and high-saturation velocity, to cite a few. Additionally, due to their ability to absorb and radiate electromagnetic waves in many frequencies, Nitride semiconductors are also technologically attractive in the LASER and LED industry. However, it is worth mentioning, at this spot, that the three-dimensional quantum confinement felt by charge carriers inside Nitride based QDs leads to the complete localization of electrons and holes and to discretizing the nanocrystal energy spectra, which increases the overlapping of electron and hole wave functions. That automatically improve the brightness of optoelectronic appliances, and gives rise to better temperature stability [15] and higher defect and radiation tolerance [16]. In this vein, the use of quantum confinement effects to control the electronic and optical properties of III-Nitride materials could pave the way for fascinating and improved devices operating in extremely hostile external mediums.

Owing to the mutual Coulomb interaction between charge carriers inside semiconductors, we are witnessing the formation of quasiparticles, otherwise known as excitonic complexes [17, 18, 19]. These quantum states play a crucial role on the optical properties of crystal materials, especially when the semiconductor dimensionality is reduced to the angstrom scale. Thus, the presentation of thorough studies concerning excitonic effects inside nanomaterials is of great interest in order to provide reliable results comparable to experimental data. To this end, various studies aimed to improve the understanding of that complicated topic were published by the past. More recently, Jansson et al. [20], using an "adapted" random population model, studied the dynamics of QDs formed in GaNAsP nano-wires. Their results show that the formation of negative trions is facilitated by the presence of hole-trap defects in the proximity to some QDs, which also brings to a clear shrink of neutral excitons lifetime. On the other hand, Elmaghraoui et al. [21] reported a theoretical approach to excitonic complexes in polar GaN/(Al,Ga)N QDs. A huge correlation was found between the binding energies of excitonic complexes in GaN/AlN and the nanodot size. Furthermore, their calculation shows that taking the exciton energy position as origin, the energy of negatively charged exciton X^- is redshifted with increasing the nanodot size, while the energy of positively charged exciton X^+ is blueshifted. The biexciton energy XX exhibits a transition from antibonding to bonding character, decreasing the neutral exciton energy. In addition, Tamariz and coworkers [22] investigated the optical properties of GaN/AlN QDs directly grown on Si(111) substrate. Their work demonstrates that these nano-systems reveal a bright single-photon sources character with count rates at the sample surface on the order of 10^6 s^{-1} at room temperature. That is explained by the large exciton binding energy in such nanocrystals. However, by the mean of atomistic calculations, Patra and Schulz [23] demonstrated that a c-plane (In,Ga)N/GaN QDs could be a choice candidate for novel non-classical light emission via twin-photon emission. Besides, Ref. [24] presents a self-consistent calculation of charged excitons inside InGaN/GaN QDs. It was established that the energy of both negatively and positively charged excitons undergoes a remarkable enhancement compared with neutral excitons energy. On the other hand, Sergent et al. [25] investigated the optical characteristics of a zinc-blende GaN/AlN QDs grown by droplet epitaxy. Their microphotoluminescence study exhibits radiative lifetimes shorter than 287±8 ps for excitonic and multi-exciton recombination. Additionally, Amloy and coworkers [26] studied the optical linear polarization properties of excitonic complexes in GaN QDs. Their results demonstrate that the polarization of the light emitted provides additional spatial information, and consequently, X and XX emissions of

individual GaN QDs could be distinguished in spectra recorded for an ensemble of nanodots.

As well known, the modulation of nanostructures morphology is among the most reliable tools to "control", to some extent, the electronic and optical characteristics of nanoscale systems, and one can find in literature several papers tackling the subject. For instance, Ref. [27] treats the size modulation of exciton binding energy in a GaN/AlN nanodot. While Williams et al. [28] investigated the change of the exciton, bi-exciton, and charged exciton energy with respect to the GaN/AlN QDs dimensionality. Further, Zheng et al. [29] examined the role of a donor impurity trap on the exciton energy for different QDs sizes and donor positions. On the other hand, Shi and Tansley [30] obtained that the impurity trap position has a significant impact on the energy of an exciton confined in strained $In_xGa_{1-x}N$/GaN QDs. Additionally, Chafai and coworkers [31] presented a theoretical study of the exciton optical characteristics change with respect to the shape of a GaSb-capped InSb heterodot. It should be noted, At this point, that the investigation of excitonic complexes inside nitride-free QDs is also extensively reported by the past, and one can refer, for instance, to Refs. [32, 34, 35, 36, 37]. However, despite the thousands of papers published about the subject, a well understanding of charge carriers interaction inside core/shell nanocrystals has still not yet occurred.

Motivated by the outstanding excitonic properties in III-Nitride based semiconductors, we tackle the problem of the binding energy size modulation of a negatively charged exciton inside a GaN/AlN type-I core/shell QD and AlN/GaN reversed type-I core/shell QD. Our theoretical model is based on a variational approach in the context of the effective-mass approximation (EMA). Further, the core-to-shell band mismatch is modeled by a finite-depth step-like potential energy in order to make our model more reliable. The organization of the paper is the following: Section II contains the presentation of the theoretical framework, in Section III, we discuss the obtained results, and in Section IV the conclusions are given.

Theoretical Framework

The understudied system consists on a negative trion, exciton in permanent Coulomb interaction with an electron, confined inside a GaN-capped AlN spherical QD. The case of negatively charged excitons inside AlN/GaN reversed type-I core/shell QD is also investigated, and a comparison between the two systems is presented in the next section. Further, it is worth mentioning that both core/shell quantum dots (CSSQD), previously introduced, are surrounded by a silica matrix, SiO_2, in order to protect them from external medium contaminations.

Figure 1 schematizes the studied nanostructures, where R_c and R_s denote, in this order, the core and shell radii, while $t_k=R_S - R_c$ stands for the shell thickness. However, U_e=1.10 eV (U_h=1.71 eV) refers to the potential barrier for electrons (holes) obtained by the means of the Anderson rule [33]. That barrier energies are highly sensitive to the electron affinity (E_{ea}), and to the HOMO-LUMO band gap (E_g) of both materials.

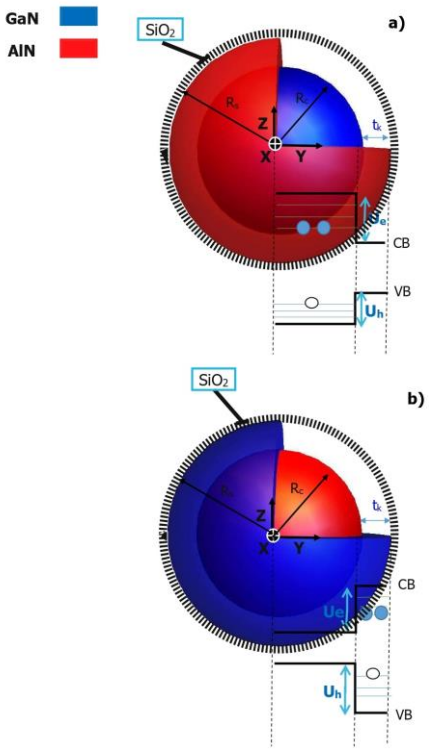

Figure 1: Schematic representation of negative trion confined inside: GaN/AlN type-I core/shell quantum dot (a) and AlN/GaN reversed type-I core/shell (b) quantum dot.

Thus, within the context of the effective mass formalism, applying the isotropic and non-degenerate parabolic approximations, taking into account the dependence of the electron effective mass on radius, and assuming that the core and shell materials dielectric constants are sufficiently close to ignore the effects of induced surface polarization charges, the

Hamiltonian of a negatively charged exciton inside a CSSQD reads:

$$H_{X^-} = \sum_{i=1}^{2}\left[\left(\frac{\hbar}{j}\nabla_i\right)\frac{1}{2\,m_{ei}^*}\left(\frac{\hbar}{j}\nabla_i\right) + U_{wei}(r_i) + \Sigma_i(R_s)\right] + \left(\frac{\hbar}{j}\nabla_h\right)\frac{1}{2\,m_h^*}\left(\frac{\hbar}{j}\nabla_h\right) + U_{wh}(r_h) + \Sigma_h(R_s) + V_{coul}\,, \quad (1)$$

where "j" stands for the "iota" imaginary number, m^*_{ei} (m^*_h) is the position dependent electron (hole) effective mass, while $U_{wei}(r_i)$ and $U_{wh}(r_h)$ are, respectively, the confinement potential of electrons and holes written, in the case of type-I GaN/AlN QDs, as:

$$U_{wei}(r_{ei}) = \begin{cases} 0 & r_{ei} \le R_c \\ U_e = 1.10\ eV & R_c < r_{ei} \le R_s \\ \infty & otherwise\,, \end{cases} \quad (2)$$

and

$$U_{wh}(r_h) = \begin{cases} 0 & r_h \le R_c \\ U_h = 1.71\ eV & R_c < r_h \le R_s \\ \infty & otherwise. \end{cases} \quad (3)$$

By contrast, the charge carriers confinement potentials inside reversed type-I AlN/GaN QDs, read:

$$U_{wei}(r_{ei}) = \begin{cases} U_e = 1.10\ eV & r_{ei} \le R_c \\ 0 & R_c < r_{ei} \le R_s \\ \infty & otherwise, \end{cases} \quad (4)$$

and

$$U_{wh}(r_h) = \begin{cases} U_h = 1.71\ eV & r_h \le R_c \\ 0 & R_c < r_h \le R_s \\ \infty & otherwise. \end{cases} \quad (5)$$

On the other hand, $\Sigma_i(R_s)$(i=e_1, e_2, e_h) stands for charge carriers self-energy taken as in Ref. [38]. The last term in Eq. (1), is the coulomb interaction expressed as follows:

$$V_{coul.} = -\frac{e^2}{\varepsilon_r(r_1,r_2,r_h)|\mathbf{r_1}-\mathbf{r_h}|} - \frac{e^2}{\varepsilon_r(r_1,r_2,r_h)|\mathbf{r_2}-\mathbf{r_h}|} + \frac{e^2}{\varepsilon_r(r_1,r_2,r_h)|\mathbf{r_1}-\mathbf{r_2}|}\,, \quad (6)$$

where $\varepsilon_r(r_1, r_2, r_h)$ is assumed to be ε_{1r} (the relative permittivity of the core material) if all charge carriers are in the core material, and ε_{2r} (the relative permittivity of the shell material) if charge carriers are in the shell material, otherwise $\varepsilon_r(r_1, r_2, r_h)=(\varepsilon_{1r}\,\varepsilon_{2r})^{1/2}$.

With the aim of calculating the energy ground state of confined negatively charged excitons, we introduced Hylleraas coordinates [39], and that leads to the following form of the Laplacian operator [41]:

$$\Delta_i = \sum_{j\neq i}\frac{2}{r_{ij}}\frac{\partial}{\partial r_{ij}} + \sum_{j\neq i}\sum_{k\neq i}\frac{r_{ij}^2 + r_{ik}^2 - r_{jk}^2}{2\,r_{ij}\,r_{ik}} \times \frac{\partial^2}{\partial r_{ij}\,\partial r_{ik}};\quad (i = e_1, e_2, h) \quad (7)$$

Against this background, the negative trion energy ground state is written as:

$$E_{X^-} = \min_{\alpha_1,\alpha_2,\beta}\left[\frac{\langle\Psi_{X^-}(\xi_{eh})|H_{X^-}|\Psi_{X^-}(\xi_{eh})\rangle}{\langle\Psi_{X^-}(\xi_{eh})|\Psi_{X^-}(\xi_{eh})\rangle}\right], \quad (8)$$

where $\Psi_{X^-}(\xi_{eh})$ stands for the negatively charged exciton trial wave function taken as:

$$\Psi_{X^-}(\xi_{eh}) = \Phi_1(r_{e_1})\,\Phi_2(r_{e_2})\,\Phi_h(r_h) \times e^{\left(-\alpha_1 r_{e_1h} - \alpha_2 r_{e_2h} + \beta r_{e_1e_2}\right)}. \quad (9)$$

ξ_{eh} denotes the set of variables on which the wave function depends: r_{e1}, r_{e2}, r_h, r_{e1h}, r_{e2h}, r_{e1e2}, where r_i (i=e_1, e_2, h) and r_{ij} (j≠i) are, in this order, the distance between the i-particle and the nanodot center and the interparticle distances. $\Phi_1(r_1)$ and $\Phi_2(r_2)$ are the ground state radial wave function of the first and the second electron respectively, chosen as in Ref. [42], while $\Phi_h(r_h)$ denotes the hole wave function taken as in Ref. [27]. However, α_1, α_2, and β are positive variational parameters, introduced in order to take into account the mutual Coulomb correlation between charge carriers.

Thus, one can define the negative trion binding energy as follows:

$$E_b = E_{X^-} - (2\,E_e + E_h)\,, \quad (10)$$

where E_e and E_h stand for, the electron and hole ground state energy, respectively.

Results and discussion

The current section provides the graphical representation of our obtained numerical results.

Table 1: The used numerical parameters [40]

	GaN	AlN	The geometric mean
Eg	3.39 eV	6.20 eV	4.58 eV
ε_r	8.9	8.5	8.69
m^*_e/m_0	0.20	0.48	0.31
m^*_h/m_0	0.26	0.47	0.35
E_{ea}	4.10 eV	3.00 eV	3.51 eV

As already mentioned, our investigation is based on a variational approach within the context of the EMA. It is pertinent to note, at this spot, that the use of Hylleraas coordinates [39], allows to reduce the degree of freedom of our confined quasi-particle from 9 to 6, which automatically simplifies the numerical calculations related to the studied nano-systems. In Table I, the various physical parameters employed in this study are outlined, where m_0 stands for the free electron mass.

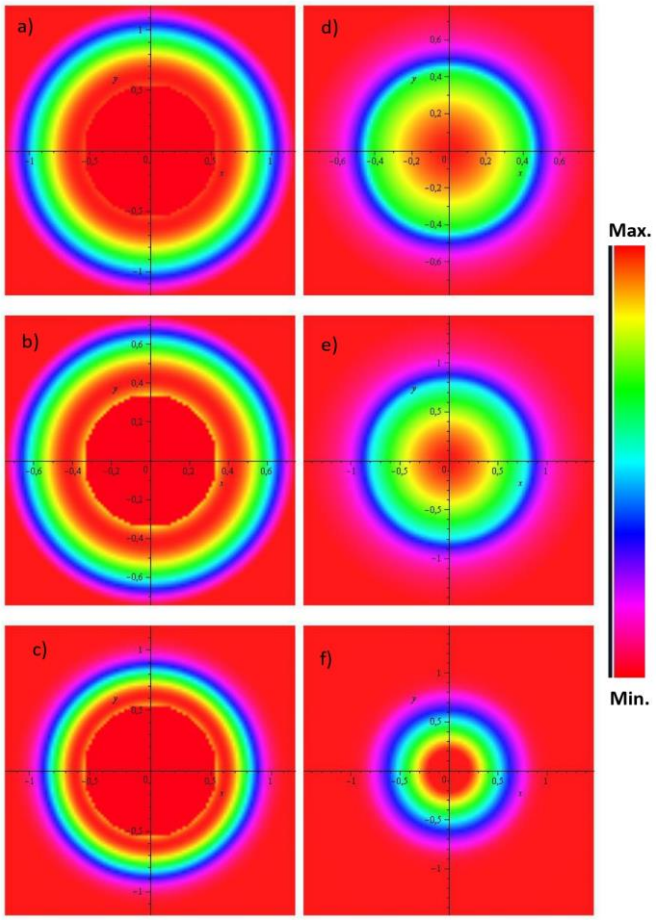

Figure 2: The radial probability density distribution of: electron inside 4.4 nm AlN/GaN QD (a), hole inside 4.4 nm AlN/GaN QD (b), trion inside 4.4 nm AlN/GaN QD (c), electron inside 4.4 nm GaN/AlN QD (d), hole inside 4.4 nm GaN/AlN QD (e), and trion inside 4.4 nm GaN/AlN QD (f). The probability density increases from red to coral. The yellow circles are the signature of the transition between regions with maximal density and those with minimal density.

Figure 2, displays the plot of the radial probability density distribution, in the x-y plane, of electrons, holes, and trions, respectively, Fig. 2a (Fig. 2d), Fig. 2b (Fig. 2e), and Fig. 2c (Fig. 2f) inside a spherical shaped AlN/GaN (GaN/AlN) core/shell nanodot with a fixed shell radius R_s=4.4 nm. It is worth noticing, that the radial probability of single particles is spherically distributed around the nanodot center for both nanocrystals, and the formation of negatively charged excitons does not break the observed spherical symmetry. Additionally, the graphs show that the probability density related to the electron, hole, and trion is maximal (coral color) near the center of GaN/AlN QD and decreases progressively when we move to the QD border. By contrast, the probability density of single particles and negative trion is virtually zero (red color) around the center of the AlN/GaN QD, and started to increase when we move far away from the center reaching its maximum value after that it starts decreasing to its minimum value (red color) near to the nanodot border. Noting that, in both core/shell nanodots, the observed yellow circles are the signature of the transition between regions in which the density is maximal and those of minimal densities. Thus, based on the aforementioned remarks, we can confirm the type-I and reversed type-I band energy alignment of GaN/AlN and AlN/GaN nanodots, respectively. In addition, one can clearly observe that the formation of negative excitonic trions, coming from the mutual Coulomb interaction between two electrons and one hole, gives rise to a trionic wave function less spread as compared with that of single particles. That is clearly related to the electrons and holes wave functions overlapping phenomenon, frequently observed in nano-sized materials.

Figure 3, shows the change of the electron energy, inside GaN/AlN QDs (Fig. 3a) and AlN/GaN QDs (Fig. 3b), as a function of the core radius and different shell thickness values. One can clearly see that, for a fixed nanodot diameter, the electron energy takes higher values in reversed AlN/GaN QDs as compared with GaN/AlN QDs, and that such behavior is observed for all the studied quantum dots sizes. This behavior is probably related to the effect of charge carriers localization inside both nanodots, which is known to be modulated by the nature of the energy level mismatch. More precisely, even for the same heterodot size, the electron wave function is either confined inside the spherical core material, GaN/AlN QDs, or in the shell region, AlN/GaN QDs, depending on the core/shell QD band alignment type. In this context, and due to the confining region shape and size, the quantum confinement effects seem to be more pronounced, although their identical morphology, inside GaN/AlN than AlN/GaN QDs, and that explains the remarkable difference observed in electron energy value. It was also observed that for a fixed shell thickness, t_k, moving the core radius from 0.005 to 1 nm decreases the electron energy in both systems. Further, we obtained that in AlN/GaN reversed type-I QDs, the electron energy stays roughly constant for R_c higher than 1 nm. By contrast, in GaN/AlN type-I QDs we assist to a slight increase in the electron energy far away R_c=1.2 nm.

Figure 4, illustrates the variation of confined hole energy, in GaN/AlN QDs (Fig. 4a) and AlN/GaN QDs (Fig. 4b), with respect to the core radius (R_c) for various shell thickness (t_k). It is worth noticing that the qualitative behavior of holes energy, is by the far, radically different from the electrons energy character. Additionally, we can observe that, as

compared to the electron energy, the confined hole energy presents very low values in both QDs. On the other hand, the qualitative behavior of confined hole energy is roughly the same in both GaN/AlN and AlN/GaN QDs. Thus, as exhibited in this figure, changing the core radius value, the shell thickness, or engineering the energy band mismatch of the confining nanosystem impact the quantitative behavior of confined hole energy. That can be certainly a reliable manner to modulate the electronic and optical properties of core/shell nanodots, paving the way for new powerful semiconductor devices.

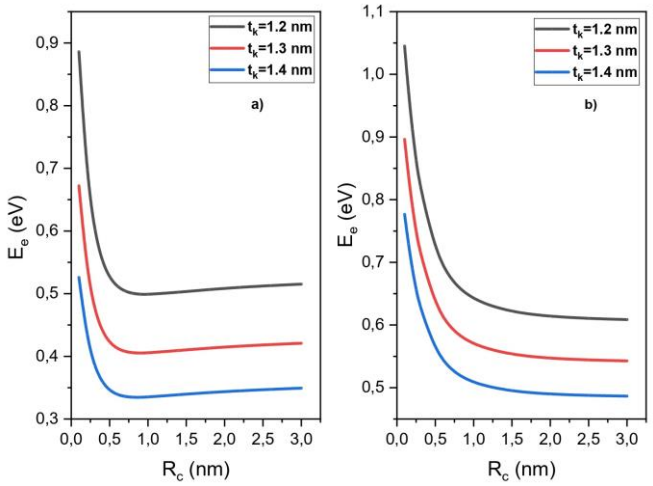

Figure 3: Electron energy as a function of the core radius for various shell thickness values tk=1.2 nm, 1.3 nm, and 1.4 nm. In (a), the results are for GaN/AlN type-I core/shell quantum dot, whereas in (b) are for AlN/GaN reversed type-I core/shell quantum dot.

Figure 5, presents the negatively charged exciton binding energy, in GaN/AlN QDs (Fig. 5a) and AlN/GaN QDs (Fig. 5b), versus the radius of the core material, R_c, for various thickness values of the shell material, t_k. It is worth noticing that, when R_c< 0.5 nm, the qualitative behavior of E_b is virtually the same in both nanodots and that is regardless of the change in the shell thickness. Otherwise, the trionic binding energy still roughly constant for AlN/GaN QDs. By contrast, as R_c moves from 0.5 nm to 3 nm, an increase E_b is observed for negative trion inside GaN/AlN QDs. One can also notice that both nanocrystals present a large trionic binding energy up to 650 meV in AlN/GaN QDs and 425 meV in GaN/AlN QDs, which literally make these systems highly attractive for application in optic and optoelectronic devices. Furthermore, we can see that the shrinking of the shell material increases the negative trion binding energy, this might be explained by increasing the localization of charge carriers ground state inside the understudied QD. Finally, one can say that the change of the nanodot size affects the localization of electrons and holes and consequently the stability of negatively charged exciton is affected. In other words, and based on the fact that quasi-particles with the highest binding energy are the more stable, there is a remarkable correlation between the overlapping of single-particle wavefunctions and the stability of negative trions. At this point, we would like to highlight that the qualitative behavior of the trionic binding energy inside AlN/GaN QDs is in perfect accordance with the experimental one obtained by Ayari *et al.* [43] of negative trion in laterally finite 2D semiconductors. Further, our results show a very enhanced negative trion binding energy with the advantage of a double control of E_b, either by changing R_c or/and t_k.

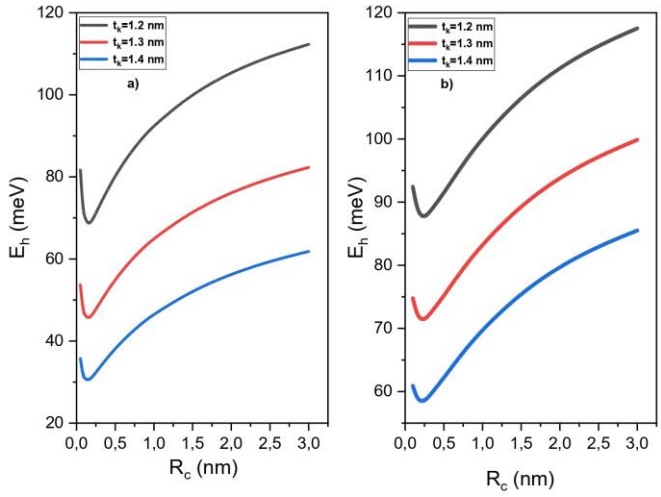

Figure 4: Hole energy as a function of the core radius for various shell thickness values t_k=1.2 nm, 1.3 nm, and 1.4 nm. In (a), the results are for GaN/AlN type-I core/shell quantum dot, whereas in (b) are for AlN/GaN reversed type-I core/shell quantum dot.

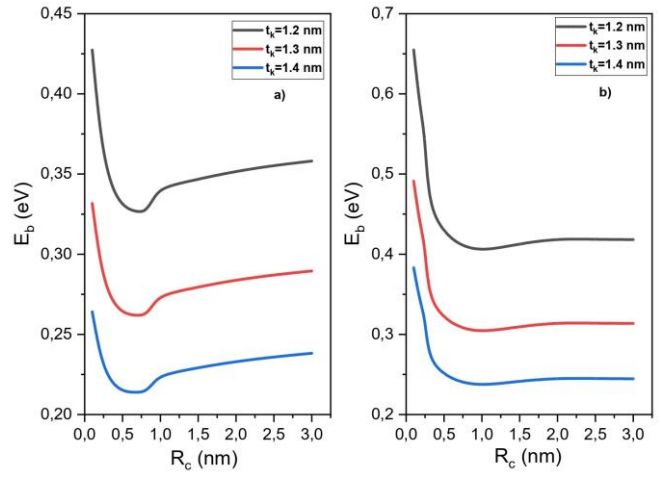

Figure 5: Negative trion binding energy as a function of the core radius for various shell thickness values t_k=1.2 nm, 1.3 nm, and 1.4 nm. In (a), the results are for GaN/AlN type-I core/shell quantum dot, whereas in (b) are for AlN/GaN reversed type-I core/shell quantum dot.

Conclusion

To sum up, the current study consists on a theoretical study of the energy behavior of electrons, holes, and negatively charged exciton confined inside nitride-based core/shell heteronanodots. Using a variational analysis, the total energy of negative trions is estimated, while single-particle energy is computed from a transcendental energy equation obtained by applying the continuity of charge carriers wavefunctions and their probability current at the core-to-shell contact surface. Our theoretical approach reveals a great correlation between the confined negative trion binding energy and the spatial parameters of the understudied quantum dots. It was also established that the nature of the core-to-shell energy band mismatch obviously affects the quantitative and the qualitative behavior of negetive trion binding energy. Furthermore, we achieved to the fact that varying the core/shell nanodot size leads us to modulate the trionic binding energy in a range extending from ~220 meV to 425 meV for GaN/AlN QDs. While for AlN/GaN QDs, the trionic binding energy can be tuned from ~245 meV to 650 meV. It is worth noting that all our data are in good agreement with the previously published papers and give a consistent interpretation of the qualitative behavior of negative trion binding energy experimentally obtained by Ayari *et al.* [43]. Additionally, one can say that the large values of E_b obtained in both nanodots, and the possibility to control this mesurable parameter in a large range, could pave the way to powerful nitride-based electronic and optoelectronic devices.

Acknowledgements:

A.A, I.E, and A.C gratefully acknowledge the support of the PPR2 project: (MESRSF-CNRST). C.A.D. acknowledges the financial support from El Patracknowledges the financial support from El Patimonio Autónomo Fondo Nacional de Financiamiento para la Ciencia, la Tecnologia y la Innovación Francisco José de Caldas (project: CD 111580863338, CT FP80740-173-2019). The authors would like to thank all the organizations.

REFERENCES

1. J. Piprek (ed), Nitride semiconductor devices: principles and simulation, John Wiley & Sons, 2007.
2. B. Gil (ed), Low-dimensional nitride semiconductors, Oxford University Press on Demand, 2002.
3. H. Morkoç, Nitride semiconductors and devices, Springer Science & Business Media, 2013.
4. M. BOSI, C. PELOSI, Prog. Photovolt.: Res. Appl. **vol.15,** p 51 (2007).
5. J. Yu, L. Wang, Z. Hao, Y. Luo, C. Sun, J. Wang Y. Han, B. Xiong, and H. Li, Adv. Mater. **vol.32**, p 1903407 (2020).
6. A. S. Adonin, A.Y. Evgrafov, Y.V. Kolkovskii, and V.M. Minnebaev, Russ. Microelectron. **vol.50**, p 197 (2021).
7. Y. Xue, H. Wang, N. Xie, Q. Yang, F.Xu, B. Shen, J.J. Shi, D. Jiang, X. Dou, T. Yu, and B.Q. Sun, J. Phys. Chem. Lett. **vol.11,** p 2689 (2020).
8. T. Vogl, R. Lecamwasam, B.C. Buchler, Y. Lu, and P.K. Lam, ACS Photonics **vol. 6,** p 1955 (2019).
9. S.T. Jagsch, N.V. Triviño, F. Lohof, G. Callsen, S. Kalinowski, I.M. Rousseau, R. Barzel, J.F. Carlin, F. Jahnke, R. Butté, C. Gies, A. Hoffmann, N. Grandjean, and S.Reitzenstein, Nat. Commun. **vol.9,** p1 (2018).
10. T.J. Lu, B. Lienhard, K.Y. Jeong, H. Moon, A. Iranmanesh, G. Grosso, and D.R. Englund, ACS Photonics **vol.7**, p 2650 (2020).
11. S.G Bishop, J.P. Hadden, F. Alzahrani, R. hekmati, D.L. Huffaker, W.W Langbein, and A.J. Bennett, ACS photonics **vol.7**, p 1636 (2020).
12. M.J. Holmes , M. Arita, and Y. Arakawa, Semicond. Sci. Technol. **vol.34**, p 033001 (2019).

13. Li Wang, X. Xu, L. Zhang, R. Qiao, M. Wu, Z. Wang, S. Zhang, J. Liang, Z. Zhang, Z. Zhang, W. Chen, X. Xie, J. Zong, Y. Shan, Y. Guo, M. Willinger, H. Wu, Q. Li, W. Wang, P. Gao, S. Wu, Y. Zhang, Y. Jiang, D. Yu, E. Wang, X. Bai, Z.J. Wang, F. Ding and K. Liu, Nature, **vol. 570**, p 91 (2019).
14. C. Elias, P. Valvin, T. Pelini, A. Summerfield, C. J. Mellor, T. S. Cheng, L. Eaves, C. T. Foxon, P. H. Beton, S. V. Novikov, B. Gil and G. Cassabois, Nature Communications, **vol.10,** p 1 (2019).
15. K. Fu, H. Fu, X, Huang, T.H. Yang, H.Chen, I. Baranowski, J. Montes, C. Yang, J.Z. and Y. Zhao, IEEE Electron Device Lett. **vol.40**, p 375 (2019).
16. R. Kikuchi, T. Nakamura, T. Kurabuchi, Y. Kaneko, Y. Kumagai, and F. Oba, Chem. Mater. **vol.33**, p 8205 (2021).
17. M. Paur, A.J.M. Mendoza, R. Bratschitsch, K. Watanabe, T. Taniguchi, and T. Mueller, Nat. Commun. vol.10, p 1 (2019).
18. X.X. Zhang, Y. You, S.Y.F Zhao, and T.F. Heinz, Phys. Rev. Lett. **vol.115**, p 257403 (2015).
19. S.Yu Chen, T. Goldstein, T. Taniguchi, K. Watanabe and J. Yan, Nat. Commun. **vol.9**, p 1 (2018).
20. M. Jha, Current Trends in Industrial Scale Synthesis of Quantum Dots and Its Application in Electronics. In : Handbook of Nanomaterials for Industrial Applications. Elsevier, (2018).
21. D. Elmaghraoui, M. Triki, S. Jaziri, G.M. Matutano, M. Leroux, and J.M. Pastor, J. Phys.: Condens. Matter **vol.29**, p 105302 (2017).
22. S. Tamariz, G. Callsen, J. Stachurski, S. Kanako, R. Butte, and N. Grandjean, ACS Photonics **vol.7,** p 1515 (2020).
23. S.K. Patra, and S. Schulz, Nano Lett. **vol.20**, p 234 (2019).
24. D.P. Williams, A.D. Andreevb, and E.P. O'Reilly, Superlattices Microstruct. **vol.36**, p 79 (2004).
25. S. Sergent, S. Kako, M. Bürger, T. Schupp, D.J. As, and Y. Arakawa, Appl. Phys. Lett. **vol.105**, p 141112 (2014).
26. S. Amloy, K.F. Karlsson, T.G. Andersson, and P.O. Holtz, Appl. Phys. Lett. **vol.100**, p 021901 (2012).
27. A. Chafai, I. Essaoudi, A. Ainane, F. Dujardin, and R. Ahuja, Physica B Condens. Matter. **vol.559,** p 23 (2019).
28. D.P. Williams, A.D. Andreev, D.A. Fauxb, and E.P. O'Reilly, Phys. E: Low-Dimens. Syst. Nanostructures, **vol.21,** p 358 (2004).
29. D. Zheng, Z. Wang, and B. Xiao, Physica B Condens. Matter. **vol.407, p** 4160 (2012).
30. Y. Chi, and J.J. Shi, Phys. Lett. A, **vol.361**, p 156 (2007).
31. A. Chafai, I. Essaoudi, A. Ainane, and R. Ahuja, Eur. Phys. J. Plus, **vol.135**, p 1 (2020).
32. N.T. Han, V.K. Dien and M.F. Lin, Sci. Rep**. vol.11,** p 1 (2021).
33. R. L. Anderson, IBM J. Res. Dev. **vol.4**, p 283 (1960).
34. A. Rawat, A. Arora, and A.D. Sarkar, Appl. Surf. Sci. **vol.563,** p 150304 (2021).
35. A. Chafai, F. Dujardin, I. Essaoudi, and A. Ainane, Superlattices Microstruct. **vol.101**, p 40 (2017).
36. A. Chafai, I. Essaoudi, A. Ainane, F. Dujardin, and R. Ahuja, Phys. E: Low-Dimens. Syst. Nanostructures **vol.101**, p 125 (2018).
37. M.H. Du, H. Shi and S. B. Zhang, J. Mater. Chem. C, **vol.7,** p 14342 (2019).

38. G. Allan, C. Delerue, and M. Lannoo, E. Martin, Phys. Rev. B **vol.52**, p 11982 (1995).

39. E.A. Hylleraas, Z. Phys. **vol.4**, p 347 (1929).

40. V.E. Borisenko, and S. Ossicini, What Is what in the Nanoworld, John Wiley & Sons, (2013).

41. A.A. Frost, Theoret. Chim. Acta (Berl.) **vol.1,** p 36 (1962) 36.

42. A. Chafai, I. Essaoudia, A. Ainanea,, F. Dujardin, R. Ahuja, Phys. E: Low-Dimens. Syst. Nanostructures **vol.104**, p 29 (2018).

43. S. Ayari, M.T. Quick, N. Owschimikow, S. Christodoulou, G.H.V. Bertrand, M. Artemyev, Iwan Moreels, U. Woggon, S. Jaziri, and A.W. Achtstein, Nanoscale, **vol.12, p** 14448 (2020).